JOURNAL OF PETROLOGY | VOLUME 46 | NUMBER 4 | PAGES 701–716 | 2005 | doi:10.1093/petrology/egh094

Solubility of Anhydrite, $CaSO_4$, in NaCl–H_2O Solutions at High Pressures and Temperatures: Applications to Fluid–Rock Interaction

ROBERT C. NEWTON AND CRAIG E. MANNING*

DEPARTMENT OF EARTH AND SPACE SCIENCES, UNIVERSITY OF CALIFORNIA LOS ANGELES, LOS ANGELES, CA 90095-1567, USA

RECEIVED DECEMBER 17, 2003; ACCEPTED OCTOBER 22, 2004
ADVANCE ACCESS PUBLICATION DECEMBER 10, 2004

Anhydrite solubility in H_2O–NaCl solutions was measured at 6–14 kbar, 600–800°C and NaCl mole fractions (X_{NaCl}) of 0–0·3 in piston–cylinder apparatus. Solubilities were determined by weight changes of natural anhydrite in perforated Pt envelopes confined with fluid in larger Pt capsules. In initially pure H_2O at 10 kbar and 800°C, $CaSO_4$ concentration is low (0·03 molal), though much larger than at the same temperature and 1 kbar. Hematite-buffered experiments showed slightly lower solubilities than unbuffered runs. $CaSO_4$ solubility increases enormously with NaCl activity: at 800°C and 10 kbar and X_{NaCl} of 0·3, $CaSO_4$ molality is 200 times higher than with pure H_2O. Whereas $CaSO_4$ solubility in pure H_2O decreases with rising T *at low* T *and* P*, the high-*P *results show that anhydrite solubility increases with* T *at constant* P *at all X_{NaCl} investigated. The effects of salinity and temperature are so great at 10 kbar that critical mixing between sulfate-rich hydrosaline melts and aqueous salt solutions is probable at 900°C at $X_{NaCl} \leq 0{\cdot}3$. Recent experimental evidence that volatile-laden magmas crystallizing in the deep crust may evolve concentrated salt solutions could, in light of the present work, have important implications regarding such diverse processes as Mount Pinatubo-type S-rich volcanism, high-fO_2 regional metamorphism, and emplacement of porphyry Cu–Mo ore bodies, where anhydrite–hematite alteration and fluid inclusions reveal the action of very oxidized saline solutions rich in sulfur.*

KEY WORDS: *anhydrite; sulfur; solubility; metamorphic brines; granulites*

INTRODUCTION

Sulfate minerals are common daughter crystals in saline fluid inclusions in rocks of deep-seated origin. Anhydrite occurs in fluid inclusions in minerals of carbonatites (Samson *et al.*, 1995), alkaline igneous rocks (Hansteen & Burke, 1990; Belkin *et al.*, 1997), Cu–Mo ores of magmatic origin (Roedder, 1984), eclogite veins in the Western Alps (Philippot & Selverstone, 1991), ultra-high-pressure coesite-bearing schists in the same region (Philippot *et al.*, 1995), and in volatile-rich melt inclusions in xenoliths in mantle-derived basalts of alkaline affinity (McInnes & Cameron, 1994). Anhydrite also forms during sulfur-rich magmatism (Luhr *et al.*, 1984; Bernard *et al.*, 1991; Streck & Dilles, 1998; Barth & Dorais, 2000; Parat *et al.*, 2002; Audétat *et al.*, 2004).

An outstanding characteristic of these occurrences is a high oxidation state, as recorded in the high Fe_2O_3/FeO ratios of the volcanic rocks (McInnes & Cameron, 1994) and in the Fe_2O_3-rich ilmenites of the Pinatubo dacites (Hattori, 1993). The great range of valence states possible in sulfur, from +6 to −2, suggests that sulfur minerals may provide an important monitor of oxidation state and, in some circumstances, may even help to control oxygen fugacity.

Several well-studied granulite–facies terranes exhibit high oxidation states on a regional scale (Griffin *et al.*, 1978; Currie & Gittins, 1988; Harlov *et al.*, 1997). Harlov *et al.* (1997) ascribed intense metamorphic oxidation of

*Corresponding author. Telephone: 1 310 206 3290. Fax: 1 310 825 2779. E-mail: manning@ess.ucla.edu

granulites of the Archean Shevaroy Hills, southern India, to the infiltration of oxidizing fluids, which left vein networks of pyrite, pyrrhotite and magnetite and caused grain-boundary alkali exchange in feldspars. They suggested migrating brines as alkali-exchanging and oxidizing agents. Widespread sulfate–carbonate scapolite in the Furua (Tanzania) granulite complex (Coolen, 1980) may indicate the action of sulfate-bearing metamorphic fluids. These rocks are also very oxidized, with Fe_2O_3-rich ilmenite present in most rocks and discrete hematite in a few. Cameron & Hattori (1994) suggested regional infiltration of SO_2-rich fluids of juvenile magmatic origin as a general cause of deep-crustal oxidation.

Disseminated anhydrite is common and sometimes abundant in the alteration zones of the Cu–Mo sulfide porphyry ore deposits of the western United States, and anhydrite is a common daughter mineral in the ultrasaline fluid inclusions in quartz associated with the highest-temperature, near-magmatic ore veins of these bodies (usually, roof zones of small granitic stocks: Roedder, 1971). The deposits are invariably highly oxidized, with ubiquitous dispersed hematite. Analogy with the Mt Pinatubo dacites suggests that widespread sulfate mineralization and high oxidation state are closely related phenomena. These sub-volcanic associations could have been influenced in their oxidation states by thermally driven downward circulation of surface waters (Norton, 1979), but several workers have emphasized that the S-rich volcanic products like those of Mt Pinatubo may result from exsolution of S-bearing gases from underlying primitive magmas (e.g. Luhr, 1990; Hattori, 1993; Hattori & Keith, 2001).

Large-scale transfer of oxidized sulfur by aqueous fluids flowing through rocks requires that sulfate must be at least moderately concentrated in the fluid. A major problem thus arises in that the solubility of anhydrite in H_2O at elevated P and T is very low. Morey & Hesselgesser (1950) found the solubility of anhydrite to be only 0·002 molal (m) at 1 kbar and 500°C. Blount & Dickson (1969) found similar low solubilities and a very strong decrease in solubility with rising temperature in this P–T range. Thus, H_2O-rich fluids, even if saturated with anhydrite, appear to be inefficient sulfur transfer agents, except perhaps in near-surface environments of high permeability.

A similar solubility problem arises in the origin of carbonated shear zones of regional extent, as in the South Tien Shan, Tajikistan (Baratov *et al.*, 1984). Middle- to high-grade alteration zones have replaced schists and gneisses with calcite, dolomite and ankerite by up to 20% in tracts of $>1000\,km^2$. The very low solubility of calcite in H_2O and H_2O–CO_2 fluids at elevated P and T (Walther & Long, 1986; Fein & Walther, 1987, 1989; Caciagli & Manning, 2003) is difficult to reconcile with the regional carbonate alteration. However, calcite is very soluble in NaCl solutions at high P and T. Newton & Manning (2002) reported a solubility enhancement of up to 40 times the pure water value (0·08 m) for concentrated NaCl solutions at 800°C and 10 kbar. Moreover, there is a very strong temperature coefficient of solubility in NaCl solutions at these P–T conditions. These extreme salinity and temperature controls on calcite solubility plausibly account for the observed regional carbonate emplacement under the hypothesis that the $CaCO_3$-bearing fluids were upward-migrating and cooling brines.

The present study explores the solubility of anhydrite in NaCl–H_2O solutions at deep-crust/upper mantle conditions (600–900°C, 6–14 kbar) to determine whether there is a large increase in solubility in saline solutions, as in calcite. Small increases occur at low P and T (e.g. Marshall *et al.*, 1964; Blount, 1965; Block & Waters, 1968; Blount & Dickson, 1969; Freyer & Voigt, 2004). Blount & Dickson (1969) measured anhydrite solubility to 1 kbar and 450°C in pure H_2O and in NaCl solutions up to 26 wt % [NaCl mole fraction (X_{NaCl}) of 0·1]. They found substantial enhancement of solubility with salinity, about 100-fold at 26 wt % NaCl. Furthermore, the strong negative temperature coefficient of anhydrite in pure H_2O is moderated and becomes slightly positive above 300°C at the highest salinity investigated. Large increases might also be expected at high P, based on the solution behavior of calcite (Newton & Manning, 2002). This is because the high degree of ionization in alkali chloride solutions at >5 kbar (H_2O densities $> 0{\cdot}7\,g/cm^3$: Aranovich & Newton, 1996) may facilitate the formation of the solute ions $CaCl^+$ and $NaSO_4^-$, which could form by reaction of $CaSO_4$ and NaCl. Furthermore, the anhydrous join $CaSO_4$–NaCl shows a deep eutectic at 1 bar with $CaSO_4$ amounting to 37 wt % of the liquid (Bergman & Golubeva, 1953). Because concentrated brines at high P and T behave more like fused salts than aqueous solutions (Aranovich & Newton, 1996), the binary fused-salt eutectic may be expected to persist into H_2O-bearing systems. Determination of a high $CaSO_4$ carrying capacity of alkali chloride solutions over a range of P, T and salinity provides insight into sulfidation, scapolitization and oxidation processes in the deeper parts of the crust and in the upper mantle.

Experimental methods

The starting material was large limpid natural anhydrite from the UCLA mineral collection (No. MS 1608). X-ray diffraction confirmed the identity of anhydrite with no extraneous reflections. The orthorhombic unit cell constants were: $a_0 = 0{\cdot}6996(2)$ nm; $b_0 = 0{\cdot}7002(2)$ nm; $c_0 = 0{\cdot}6239(2)$ nm. These constants agree, within uncertainties, with the ASTM data (No. 37-1496) for synthetic anhydrite. Energy dispersive analyses indicated that

the only detectable departure from $CaSO_4$ chemistry was SrO < 0·5 wt %.

The experimental procedure used in this study was nearly identical to that used by Newton & Manning (2002) for calcite solubility. Briefly, crystals of a natural anhydrite sample were heated in air at 400°C for 20 min to purge any volatiles. Anhydrite grains, weighed amounts of deionized H_2O and reagent NaCl were then sealed by arc-welding into Pt capsules of 3 mm diameter and 0·15 mm wall thickness. The anhydrite was encased in an inner Pt tube of 1·5 mm diameter and 2 mm length, lightly crimped at the ends and perforated with 6–10 small holes to allow access of fluids. The solubility at the highest temperatures and most concentrated NaCl solutions proved to be too high for this simple technique, and either larger unencapsulated crystals were used, or additional powdered anhydrite was added to the outer capsule to presaturate the fluid. The latter method assumes that finely divided anhydrite dissolves much faster than the large, Pt-encased single crystals—an assumption that appears to be justified by the solubility behavior.

All experiments were done with the 1·91 cm diameter piston–cylinder apparatus with NaCl pressure medium and graphite heater sleeve. The pressure chamber was highly polished WC with a no-tolerance piston fit. The Heise Bourdon tube pressure gauge was calibrated against a highly precise 1000 bar Heise gauge of 40 cm dial diameter. The two gauges read the same in the range 0–300 bar (equivalent to 0–9 kbar sample pressure) to within 1 bar, with no systematic discrepancy or hysteresis. Temperatures were controlled automatically and measured with calibrated matched pairs of W–3%Rh vs W–25%Rh thermocouples. A typical thermoelement was compared with a certified Pt vs Pt–10%Rh thermocouple in a test piston–cylinder assembly identical to those of the solubility experiments. The two thermocouple junctures were less than 0·2 mm apart, though mutually insulated. The test was made at 10 kbar and 600–800°C. The Pt–Rh thermocouple read consistently 1°C lower at 800°C than the W–Re thermocouple, which was the control element. Precision of measurements is conservatively estimated at ±300 bars sample pressure and ±3°C.

Solubility determinations were made from the weight losses of inner Pt capsules or unencapsulated anhydrite crystals. Weights were determined on a Mettler M3 microbalance at a precision of 2 μg (1σ) based on repeated weighings over the course of this study. Quenched and cleaned sample capsules generally showed negligible weight changes from the starting values, indicating no loss of material from the capsules during the experiments. The H_2O of the charges was redetermined by a puncture and drying technique, which confirmed the weighing-in values within 0·3%. The drying weight loss was taken to be the H_2O content of the experiment.

Previous investigations of anhydrite solubility have not considered a possible effect of variable oxygen fugacity (fO_2). The measurements of Blount & Dickson (1969) were self-buffered, in the sense that the solute sulfate would have reacted with H_2O to form small amounts of H_2S, with the release of O_2, resulting in a rather high, but unknown, fO_2. In the present study, in addition to the unbuffered runs, we measured the solubility of anhydrite in initially pure H_2O at 10 kbar and 800°C using internal buffer capsules containing hematite + magnetite, NiO + Ni metal, or $MnO_2 + H_2O$ (10–12 mg solid and 2–3 mg H_2O) enclosed in small welded Pt tube segments. The buffer capsules were sealed with encapsulated anhydrite crystals and about 36 mg H_2O in the outer Pt jackets. The buffered runs were made over periods of 5–40 h to test the degree of equilibration of the fluids with the internal buffers, and to investigate the variation in solubility with fO_2.

EXPERIMENTAL RESULTS

Experimental results are given in Table 1. Measurable solubility was detected at all P, T and X_{NaCl} investigated. A single experiment (No. 14, Table 1) was performed to control for S loss to Pt encapsulating materials by loading an empty inner capsule along with anhydrite powder and H_2O. The empty inner capsule showed no detectable weight change, indicating that measured weight changes can be ascribed entirely to anhydrite dissolution.

Large weight losses in experiments on NaCl-rich compositions indicated very high solubilities. These experiments yielded complex textures of quench material along with the residual crystal(s). Halite–anhydrite intergrowth textures in the dried former fluid phase were examined with the polarizing microscope, scanning electron microscope and X-ray diffraction. A regular box-work of large, thin anhydrite quench-crystals and interstitial halite (Fig. 1a) shows that the anhydrite formed first in the quench, with subsequent co-precipitation of anhydrite and halite. X-ray diffractograms of the dried quench material showed only halite and anhydrite. D-spacings of the quench anhydrite were identical to those of the starting material. Residual starting crystals retrieved from NaCl-rich experiments were sometimes solution-rounded flat bars (Fig. 1b) which could be easily separated from the quench material for weighing, but often there was recrystallization into many smaller crystals, which were harder to identify and separate. For this reason, the majority of the NaCl-rich experiments used encapsulated single crystals together with external powdered anhydrite to presaturate the fluid phase.

Table 1: Experimental results

Expt. number	Temperature (°C)	Pressure (kbar)	Duration (h)	Anhydrite (mg)	Capsule (mg)	NaCl (mg)	H_2O (mg)	X_{NaCl}	H_2O out (mg)	Capsule out (mg)	Anhydrite out (mg)	Solubility (molal)	Notes
Unbuffered experiments													
10	600	10	136	2·045	58·370	0·000	34·283	0·000	34·323	58·300		0·015	Outer capsule embrittled; white needles in inner capsule
21	600	10	60	3·297	75·367	11·159	31·741	0·098	31·599	73·970	1·878	0·325–0·330†	
23	600	10	64	5·321	77·573	20·918	26·555	0·196	26·428	74·948	2·459	0·730–0·795†	
20	600	10	65	4·084 + 2·631*	71·590	28·623	20·492	0·301	20·470	70·095	2·363	1·481–1·562†	
8	700	10	71	1·517	64·379	0·000	29·737	0·000	29·793	64·300		0·019	
13	700	10	65	4·632	77·072	10·660	30·064	0·099	29·926	74·983		0·513	
19	700	10	62	4·375 + 3·432*	81·954	21·152	26·495	0·197	26·364	80·430	2·488	1·381–1·482†	
4	700	10	68	2·773	u	26·680	19·895	0·292	17·590		0·000	>1·158	Outer capsule oozed in loading; weights corrected for NaCl loss
12	700	10	40	10·282	u	27·310	19·597	0·300	19·499		2·288	3·011	
30	800	10	6	0·743	75·682	0·000	36·050	0·000	36·116	75·583	0·585	0·020–0·032†	
6	800	10	18	1·950	69·175	0·000	32·212	0·000	32·263	69·063	1·803	0·025–0·033†	
32	800	10	34	0·530	72·030	0·000	38·454	0·000	36·567	71·951	0·367	0·016–0·033†	White rosettes (gypsum?) in inner capsule
17	800	6	20	5·018	79·401	11·050	30·642	0·100	30·999	76·820	2·272	0·612–0·651†	
15	800	10	20	7·939	u	13·088	33·502	0·107	33·700		3·245	1·023	
16	800	10	24	4·194 + 2·172*	72·651	10·747	31·304	0·096	30·549	70·974	2·462	0·925–0·935†	
18	800	14	26	4·525 + 2·709*	74·496	10·994	29·400	0·103	29·338	71·777		1·359	
22	800	10	21	4·150 + 8·241*	71·183	20·660	25·138	0·202	25·252	69·770	2·351	2·808–2·920†	
5	800	10	39	8·167	u	29·459	20·138	0·311	20·171		0·000	>2·974	
7	800	10	20	20·540	u	33·695	24·411	0·298	24·541		2·423	5·423	
14	800	10	38	4·526	31·951	0·000	34·469	0·000	33·535	31·955			Blank test for sulfidation of Pt
Buffered experiments													
28	800	10	20	2·251	51·101	0·000	35·766	0·000	36·206	50·349		0·153	NNO buffer; strong H_2S odor
29	800	10	5	1·008	73·572	0·000	35·734	0·000	35·784	73·499	0·937	0·015	HM buffer
27	800	10	19	2·418	47·365	0·000	34·319	0·000	34·339	47·280	2·365	0·018–0·011†	HM buffer
33	800	10	43	0·918	68·851	0·000	36·376	0·000	36·413	68·773	0·830	0·016–0·018†	HM buffer
31	800	10	18	0·432	70·837	0·000		0·000	35·721	70·768		0·014	MnO buffer

Explanation: 'in' and 'out' refer respectively to weights before and after experiment. H_2O out was used in all solubility calculations (see text). 'u' signifies that anhydrite crystal was unencapsulated. Blank entries indicate that measurement could not be made. 1σ uncertainty in solubility determinations is 0·001 molal, based on propagated weighing errors of ±0·002 mg per weighing step; 1σ in $X_{NaCl} < 2{\cdot}3 \times 10^{-4}$. HM, hematite–magnetite; MnO, Mn_2O_3–MnO_2 buffer; NNO, Ni–NiO.

*First weight refers to anhydrite single crystal, second weight to anhydrite powder added to outer capsule.

†Range in solubility due to minimum from capsule weight change and maximum from crystal weight change (see text).

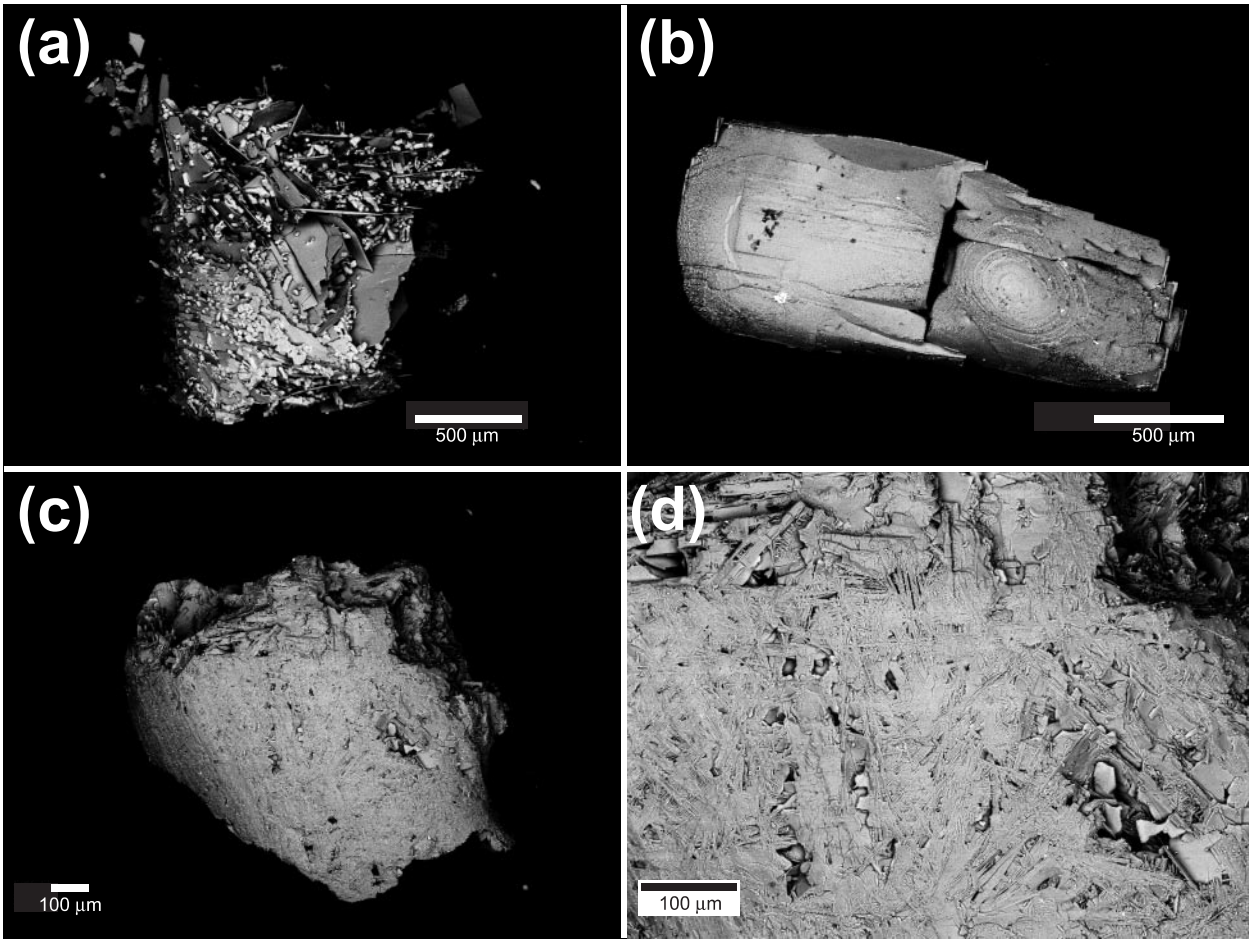

Fig. 1. Back-scattered electron microscope images of quenched charges. (a) Portion of dried fluid phase from run at 800°C, 10 kbar, $X_{NaCl} = 0{\cdot}3$ (run 7, Table 1)—large-bladed anhydrite quench crystals in parallel arrays with interstitial halite and smaller anhydrite. Halite partially dissolved away in upper portion. (b) Residual anhydrite starting material (run 22, 800°C, 10 kbar, $X_{NaCl} = 0{\cdot}2$)—originally two angular cleavage fragments, now grown together and solution-rounded. The oval striations are solution-etched cleavage planes that define 'contours' on a domed surface. (c) Bead of quenched molten anhydrite from run 28 (800°C, 10 kbar, initially pure H_2O, Ni–NiO buffer). (d) Magnification of C, showing anhydrite quench-laths.

Quenched NaCl was dissolved from the inner capsules by soaking in water at 90°C for periods of 10 min followed by drying, until a capsule came to constant weight. This treatment did not remove the small amount of quench anhydrite from the inner capsule, so that the final weight gave a lower limit to the solubility. The inner capsule was cut open and the contents were transferred to a Pt weighing pan. The quench anhydrite was texturally distinct and could be separated with a needle, but this treatment usually resulted in the loss of a small amount of granular anhydrite. The weight of the residual crystals therefore returned an upper limit for solubility. The lower and upper limits so determined define a range within which there is uniform probability of finding the solubility of anhydrite.

Figure 2 plots the solubilities from the HM-buffered and unbuffered runs with initially pure H_2O. The time required for equilibration with the buffers was at most 10 h. The run of 18 h with the MnO_2 buffer (run 31, Table 1) gave the lowest solubility. The capsules of buffering material retained H_2O without detectable weight loss and all members of the buffering assemblages were still present. The MnO_2 buffer material was coarsely recrystallized to dominant pyrolusite and subsidiary bixbyite (Mn_2O_3). Extrapolation of low-T thermodynamic data for pyrolusite suggests that fO_2 in these experiments was above HM.

Solubilities in experiments with initially pure H_2O at 10 kbar are low, in the range 0·01–0·03 m, and increase slightly with T (Table 1). Runs at 800°C and 10 kbar with HM and MnO_2 buffers show a minor, probably real, decrease of solubility with increase of fO_2, though the uncertainty limits of the measurements overlap. The NNO experiment (run 28, Table 1) showed greatly

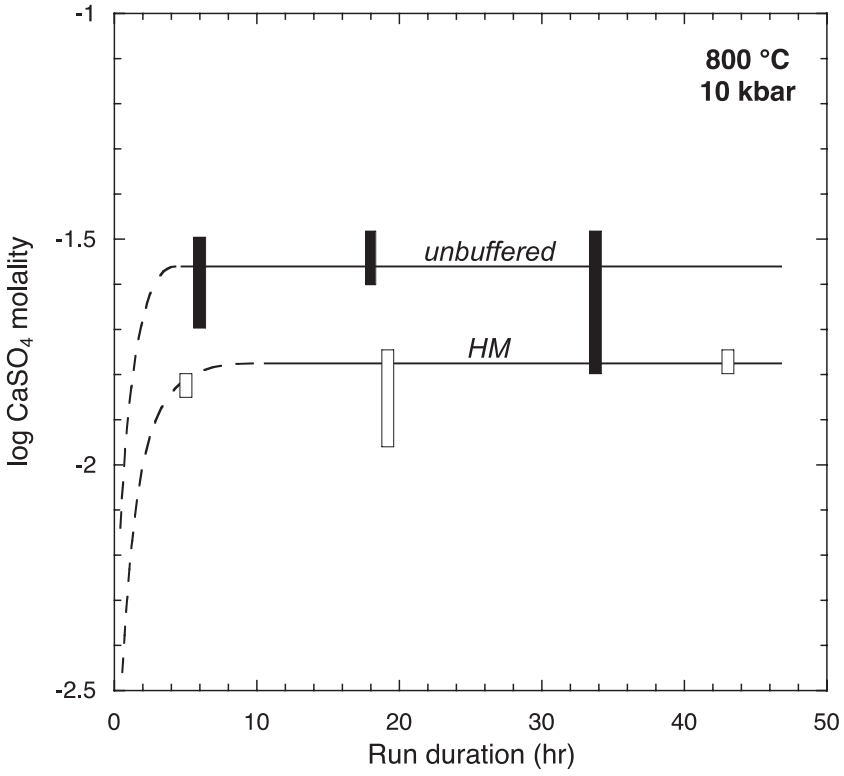

Fig. 2. Anhydrite solubility (mol/kg H_2O) at 800°C, 10 kbar, initially pure H_2O, as a function of time. Oxygen fugacity was either unbuffered, or buffered at hematite–magnetite equilibrium (HM). The lack of significant change in solubility with time in each set of experiments indicates attainment of equilibrium. The data show that solubility is lower in HM-buffered experiments than in unbuffered runs.

different behavior. The capsule emitted a strong H_2S odor when punctured. The inner capsules and the inside of the outer capsule were darkened, probably indicating reaction to PtS. The content of the inner sample capsule was a rounded bead (Fig. 1c) showing the imprint of machining striations from the Pt. Higher-magnification examination (Fig. 1d) showed the bead to be a mass of skeletal crystals; the anhydrite had been melted. The tabular habit of the anhydrite quench crystals was quite similar to that quenched from the NaCl-rich runs. The solubility in the NNO-buffered run was substantially higher than in the high-fO_2 experiments, although some of the apparently high solubility may result from loss of S to the Pt capsule.

Figure 3 shows results of 10 kbar NaCl-bearing experiments. Run durations of >60 h at 600°C to >20 h at 800°C were assumed to be adequate to ensure equilibrium in view of results in pure H_2O (Fig. 2), and the fact that Blount & Dickson (1969) demonstrated attainment of equilibrium in 24 h at 400°C. The experiments show that anhydrite solubility increases significantly with X_{NaCl} at all T. For example, anhydrite is quite insoluble in pure H_2O at 800°C and 10 kbar, but 30 mol % NaCl in the fluid raises the solubility by a factor of nearly 200. This anhydrite-saturated solution has the composition 27 wt % $CaSO_4$, 42 wt % NaCl, 31 wt % H_2O.

The solubility data of the NaCl-present experiments from 6 to 14 kbar (Table 1) can be systematized by a general expression of the form $\log [m(CaSO_4) - m_0(CaSO_4)] = a + b \log X(NaCl)$, where a and b are functions of P and T (in kbar and Kelvins, respectively) and m_0 is the molality in pure H_2O. An excellent fit to the data could be achieved by functions of the forms $a = a_1 + a_2T$ and $b = b_1 + b_2T + b_3(P - 10)$. Regression of the experimental data gave the constants $a_1 = -1{\cdot}533$, $a_2 = 0{\cdot}00291$, $b_1 = 1{\cdot}441$, $b_2 = 0{\cdot}000160$, $b_3 = -0{\cdot}0413$. Figure 3 also shows regressed and extrapolated solubility curves.

DISCUSSION

The solubility behavior of anhydrite is analogous to that of calcite (Newton & Manning, 2002; Caciagli & Manning, 2003) in several respects. Both solutions show marked decrease of solubility with rising temperature at low pressure (Fig. 4), with vanishingly small solubilities at 1 kbar and >600°C. Solubility increases by several orders of magnitude with pressures to 10 kbar in this

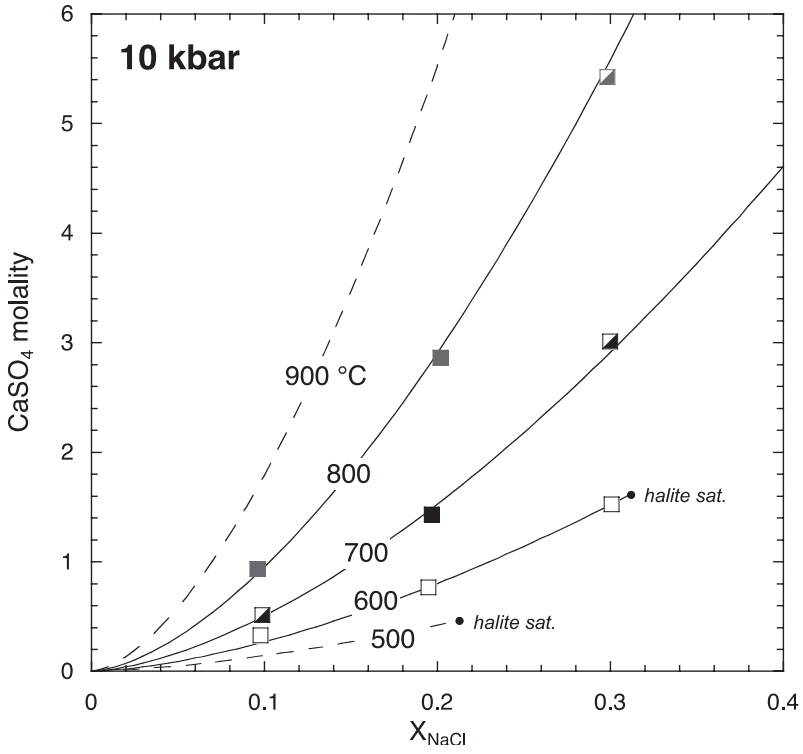

Fig. 3. Anhydrite solubility data in NaCl solutions at 10 kbar. The range in solubility constrained by minimum and maximum values (Table 1) is smaller than the symbol size. Partially filled squares indicate solubility is a minimum only; however, maximum values are never more than 10% above minima at $X_{NaCl} \geq 0{\cdot}1$ (Table 1). Accordingly, minimum values were also used to constrain fitted solubility curves (continuous lines; see text). Dashed curves are extrapolations of the regression equation to 500 and 900°C. The isothermal curves are terminated by halite saturation (filled circles). The enormous increase in anhydrite solubility with NaCl concentration is evident. The predicted increase at 900°C is so large that critical mixing between hydrosaline melts and concentrated salt solutions may be expected in the neighborhood of $X_{NaCl} = 0{\cdot}3$.

temperature range, and the temperature coefficient of solubility becomes positive for both $CaCO_3$ and $CaSO_4$. Both oxysalts show great solubility enhancement in NaCl solutions, which undoubtedly follows from the high solubility of $CaCl_2$ as a reaction product.

Caciagli & Manning (2003) showed that aqueous CO_2 is the dominant carbon species when calcite dissolves at high pressure. By analogy, the neutral species H_2S and SO_2 are likely to be the dominant sulfur products of anhydrite dissolution in initially pure H_2O. These volatile species are generated by the reactions

$$CaSO_4 + 2H_2O = H_2S + Ca^{2+} + 2OH^- + 2O_2 \quad (1)$$

and

$$2CaSO_4 + 2H_2O = 2SO_2 + 2Ca^{2+} + 4OH^- + O_2. \quad (2)$$

These reactions reveal that the solubility of anhydrite (i.e. the concentration of Ca^{2+}), as well as the H_2S/SO_4 ratio in the solution, depends strongly on the oxygen fugacity.

Figure 5 shows equilibrium concentrations of solute species in the system $CaSO_4$–H_2O as calculated at 5 kbar and 800°C by simultaneous solution of mass action, mass balance, charge balance and activity coefficient (Davies, 1962) equations for the species shown. Only species present at $>10^{-6}$ molal were considered (except H^+). It can be seen that total Ca and S concentrations (i.e. anhydrite solubility) decrease with increasing fO_2, as indicated by experimental results at higher P (Table 1). Figure 5 also shows a representation of the present 800°C, 10 kbar solubility data at a range of fO_2. Translation of the anhydrite solubility curve from 5 to 10 kbar suggests that the unbuffered runs had fO_2 above the H_2S–SO_2 equivalence point but below HM. The unbuffered measurements indicate that $CaSO_4$ is a strong oxidizing agent in a nominally closed system with H_2O.

The present pure H_2O data are not sufficient to define anhydrite solubility as a function of fO_2 at all P and T studied. However, the enhancement effect of NaCl dwarfs any effect of fO_2, as shown in Fig. 3. The 10 kbar isothermal solubility curves are approximately quadratic, implying a solvent dissolution reaction similar to

$$\underset{\text{anhydrite}}{CaSO_4} + 2NaCl = CaCl_2 + Na_2SO_4. \quad (3)$$

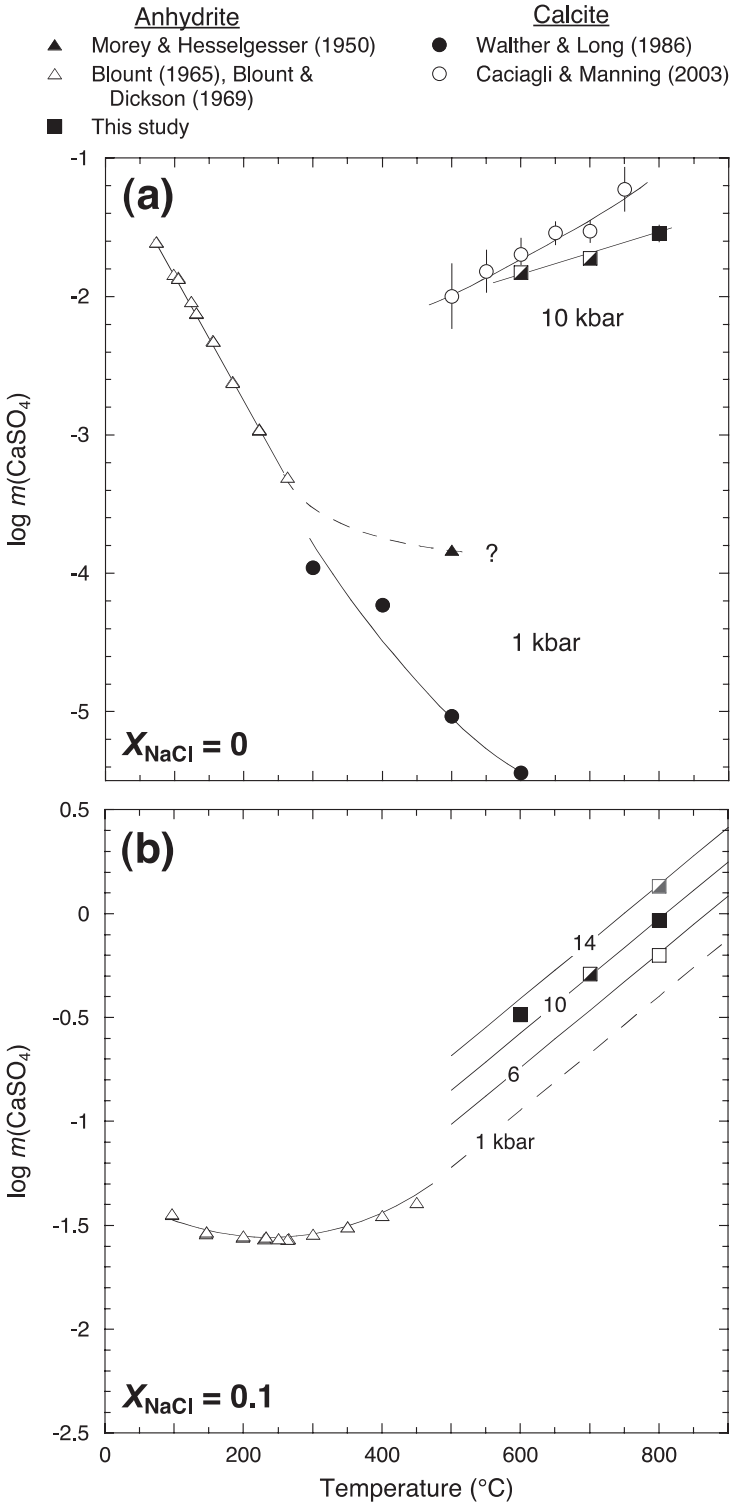

Fig. 4. Comparison of the solubility of anhydrite at ≥600°C and ≥6 kbar (squares; this study) with previous results at 1 kbar and lower T (triangles; Morey & Hesselgesser, 1950; Blount, 1965; Blount & Dickson, 1969) at $X_{NaCl} = 0$ (a) and 0·1 (b). Partly filled squares indicate that value is minimum (see Fig. 3 caption). In (a), all lines are fitted by eye. The solubility behavior of $CaSO_4$ in pure H_2O is similar to that of $CaCO_3$ (circles) at 1 kbar (Walther & Long, 1986) and at 10 kbar (Caciagli & Manning, 2003). In (b), the continuous lines connecting data from the present study are from the empirical formula given in the text. Our extrapolated curve at 1 kbar and $X_{NaCl} = 0{\cdot}1$ (dashed line) agrees well with the 1 kbar data of Blount (1965) and Blount & Dickson (1969) at lower temperatures (fitted by eye).

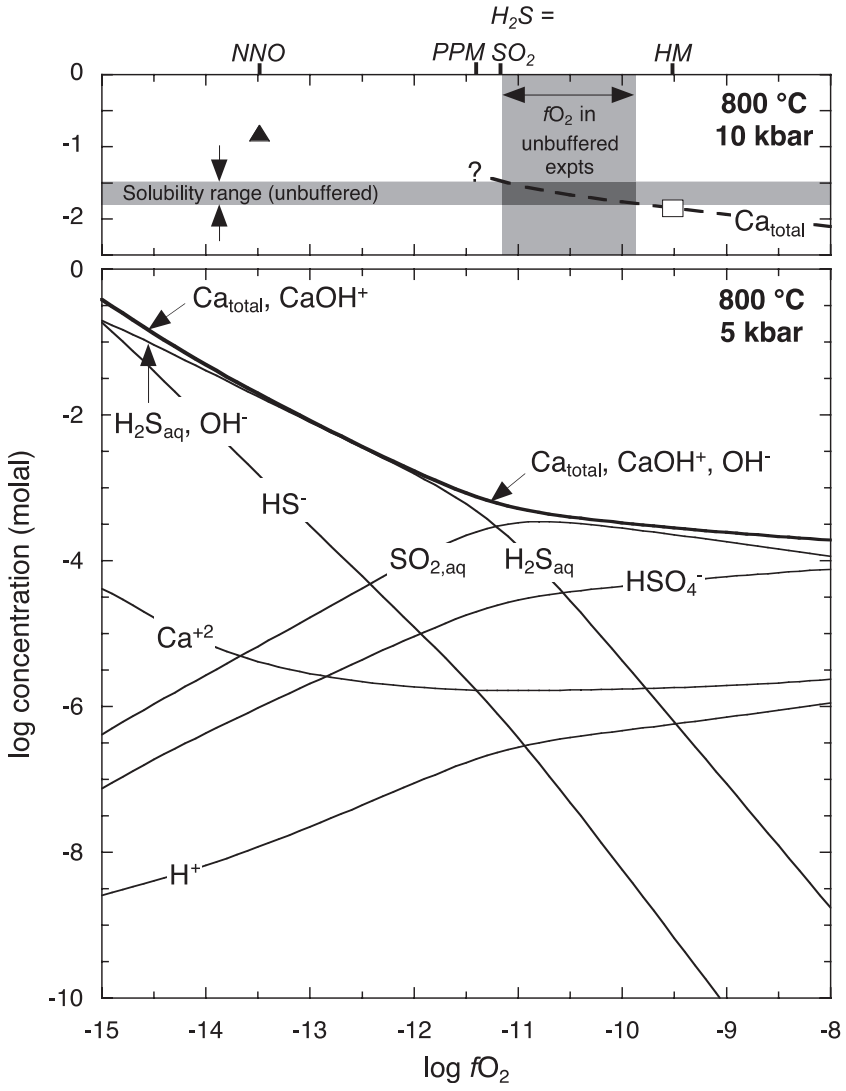

Fig. 5. Anhydrite solubility in H_2O as a function of fO_2, as calculated at 800°C, 5 kbar (lower panel) and measured at 10 kbar (upper panel). Calculations at 5 kbar were carried out using SUPCRT92 (Johnson *et al.*, 1992) and data from Helgeson *et al.* (1978) for minerals and Shock *et al.* (1989, 1997) for aqueous species. $SO_{2,aq}$ and H_2S_{aq} were used rather than the corresponding gas molecules. S and Ca species other than $SO_{2,aq}$ and H_2S_{aq}, HS^-, and HSO_4^- were ignored because relevant pK values predicted very low concentrations. Standard states were unit activity of the pure phase at any T and P for minerals and H_2O, and unit activity of the hypothetical 1 *m* solution referenced to infinite dilution for aqueous species. Activity coefficients of charged species were calculated using the Davies (1962) equation; activity coefficients of neutral aqueous species were taken to be unity. Predicted concentrations were generated by simultaneous solution of mass action, mass balance, charge balance and activity coefficient expressions. Anhydrite solubility (bold line), which is equivalent to total Ca and S concentrations, is a strong function of fO_2. Concentrations of individual aqueous species are shown with light lines, and all vary with fO_2. Solutions are basic over the range of fO_2 examined, leading to predominance of $CaOH^+$ over Ca^{2+}. The upper panel shows experimental results at 10 kbar at the NNO (triangle) and HM (rectangle) buffers. Values of log fO_2 corresponding to NNO, HM, PPM (pyrrhotite–pyrite–magnetite) buffers are shown at the top, along with the equivalence point for H_2S–SO_2. The range of fO_2 in unbuffered experiments (vertical gray band) was estimated from the intersection of the experimental solubility range (horizontal gray band) with the anhydrite solubility curve (bold dashed line), which was assumed to have the same dependence on fO_2 as at 5 kbar at high fO_2 and to intersect the midpoint of the solubility range constrained by the HM experiment. This suggests that log fO_2 in unbuffered experiments was between −9·9 and −11·2.

The salts on the right-hand side are very soluble, which tends to drive the reaction to the right. The above reaction is analogous to that deduced by Newton & Manning (2002) for calcite solution in NaCl solutions, though the NaCl enhancement for $CaSO_4$ is five times as great as for $CaCO_3$ at 10 kbar. The temperature coefficient of solubility at constant X_{NaCl} is very large, as for calcite. Figure 3 shows the predicted 10 kbar

solubility curves at 500 and 900°C. The solubility at 900°C is so large that the fluids are best regarded as supercritical hydrosaline melts or fused salt mixtures. For instance, an anhydrite-saturated fluid at 10 kbar, 900°C and $X_{NaCl} = 0{\cdot}3$ is predicted to contain 38 wt % $CaSO_4$, 36 wt % NaCl and 26 wt % H_2O.

PETROLOGICAL APPLICATIONS

High-S volcanic eruptions

The andesite–dacite eruption of Mt Pinatubo, Philippines, in 1991, released great quantities of oxidized sulfur to the atmosphere. The finding of anhydrite in the dacite tephra ejected by this eruption (Bernard *et al.*, 1991) has led to much discussion of the role of oxidized sulfur in subduction zone volcanism. Studies of anhydrite occurrence at Mt Pinatubo (Hattori, 1993) and in the tephra of the recent eruptions of El Chichón, Mexico (Luhr *et al.*, 1984) and Nevado del Ruiz, Colombia (Melson *et al.*, 1990) have emphasized their similarities, especially with respect to the high oxidation states shown by the tephra. Experimental studies on the stability of anhydrite in the crystallization of andesite (Luhr, 1990) and dacite (Scaillet *et al.*, 1998) indicate that quite high oxygen fugacity, from 1 to 3 log units above the nickel–nickel oxide buffer, is required to stabilize anhydrite relative to sulfides at magmatic temperatures (750–1000°C) and upper-crustal pressures (1–4 kbar).

The source of the sulfur in high-S volcanism could be ophiolite sulfide deposits or anhydrite-bearing evaporite beds, either in the source regions of the magmas, or scavenged by the magmas in transit. The former source does not provide an oxidation mechanism and the latter source, proposed by Rye *et al.* (1984) for El Chichón on the basis of evaporite beds of Mesozoic age underlying this volcano, would not be appropriate for Mt Pinatubo, which has no underlying evaporite stratigraphy (Imai *et al.*, 1996). The most probable source of sulfur in these eruptions was primitive mafic magmas which transferred sulfur to more evolved magmas and crustal melts (El Chichón: Luhr, 1990; Nevado del Ruiz: Melson *et al.*, 1990; Pinatubo: Pallister *et al.*, 1992). Pallister *et al.* (1992) postulated a 'basalt trigger' for the eruption process.

Luhr *et al.* (1984) pointed to a mass-balance problem arising from the high-S contents of the El Chichón tephra: experiments by Carroll & Rutherford (1987) on S solubility in a basaltic magma at 2 kbar show a maximum of about 800 ppm, and this occurs at very high oxygen fugacity. According to Luhr *et al.* (1984), the >2 wt % of S of some of the El Chichón rocks could never have been dissolved in a magma of the rock composition, but must have been introduced by a fluid phase that interacted with the partially solidified magma and that deposited anhydrite. Hattori (1993) came to the same conclusion for the anhydrite-bearing dacite tephra of Mt Pinatubo. Those workers and Gerlach *et al.* (1996) envisioned a C–O–H–S magmatic gas as the agent of sulfur transfer. A fluid-transport mechanism for anhydrite emplacement in the Mt Pinatubo tephra was confirmed recently by scanning electron microscopy, which revealed etch pits and growth features diagnostic of fluid deposition (Jakubowski *et al.*, 2002).

The present work suggests an alternative mechanism of fluid-mediated S transfer. The experiments of Kilinc & Burnham (1972) on Cl solubility in granitic melts and those of Webster *et al.* (1999) in basaltic and andesitic magmas show that, at pressure greater than near-surface conditions, a saline solution, rather than a Cl_2-bearing gas, would probably be evolved during crystallization of a hydrous Cl-bearing basalt magma. Concentrated brines have been identified as primary fluid inclusions in alkali-rich volcanic and plutonic rocks (Frost & Touret, 1989; Lowenstern, 1994). At 2–4 kbar and 1000°C, a NaCl solution could contain up to a few weight percent of sulfate, depending on the salinity. For instance, a mildly saline aqueous fluid having 5 mol % NaCl would have, at 1000°C and 4 kbar, an anhydrite saturation $CaSO_4$ molality of 0·495, or 5·4 wt %, based on the present data. Because of the large temperature coefficient of anhydrite solubility, cooling to 800°C (0·143 *m*) would precipitate most of the $CaSO_4$. Thus, a substantial amount of anhydrite could be delivered to the host rocks, even for small fluid/rock ratios.

An important consideration is whether the anhydrite of the Mt Pinatubo dacites is simply a monitor of generally high oxidation state of the magmatism or whether fluid-transported sulfur undergoes spontaneous changes in oxidation state in cooling and reaction with country rocks such that it becomes an oxidizing agent after release from a basaltic magma source. The latter point of view was argued by Hattori (1993), who pointed to a greatly increased stability of H_2S in cooling of a C–O–H–S fluid from basalt magma temperatures. Oxygen liberated from the conversion of SO_2 to H_2S would oxidize ferrous iron in the partially molten dacite envelope and stabilize anhydrite.

Hattori (1993) envisioned a reduced and relatively dry basaltic source of the sulfur-bearing fluid. However, a sufficiency problem remains with this hypothesis: sulfur solubility in basalt magma would be at a minimum at low oxygen fugacity and low H_2O activity, which would therefore require that the external S-rich dacites react with very large volumes of fluid expelled from the basalts, the majority of the S remaining in the fluid as H_2S. If, on the other hand, the basaltic source magma was originally hydrous and highly oxidized, then, according to the measurements of Luhr (1990), the magma could contain a high sulfate content: 0·5 wt % S at 1000°C and 4 kbar, steadily increasing with pressure. A subduction-zone-derived basaltic magma could have

been initially very oxidized and sulfur-rich. The fluid separating from this magma would have been initially in oxidative equilibrium with the magma and therefore also very oxidized. High oxidation state would favor the partitioning of S into the evolving fluid phase. From this point of view, emplacement of anhydrite in the surrounding rocks would seem to be more an indicator of a fundamentally high oxidation state of the magmatism than an oxidizing mechanism. It should be pointed out, however, that SO_2- or sulfate-bearing fluids can conceivably increase somewhat in oxidation state by sulfidation reactions in country rocks or derivative magmas that the fluids traverse while cooling. Hattori (1993) found petrographic evidence of pyrrhotite emplacement in the Pinatubo dacites at an early stage of metasomatic alteration. Conversion of SO_2 to H_2S in the fluid could account for some additional oxidation of host rocks if fluid fluxes were large.

Pasteris *et al.* (1996) discovered brine inclusions in quartz crystals from Mt Pinatubo tephra. Some of these inclusions contain halite and anhydrite daughter crystals, indicating that extremely concentrated, S-rich saline fluids coexisted with partially molten dacites at a pre-eruptive stage. This information, together with Luhr's (1990) experimental evidence for the existence of more primitive parental magmas, rich in sulfur and highly oxidized, with the experimental evidence for the important role of Cl in the early outgassing of mafic magmas (Webster *et al.*, 1999), and with the present finding of the high carrying capacity for sulfate of Cl-rich aqueous fluids at high T and P, leads to the conclusion that concentrated and oxidized brine, expelled from deep-seated mafic magmas, should be considered as a medium for anhydrite deposition and oxidation in S-rich volcanism.

Oxidized granulites

Several workers have suggested that the source of heat for granulite-facies metamorphism may be commonly or principally deep-crustal intrusions of mantle-derived ('underplated') magmas (Bohlen, 1987; Harley, 1989). Until recently, advocates of underplating have not examined the possibility that infiltration of magma-derived Cl-rich and perhaps S-rich supercritical fluids, analogous to those discussed in the preceding section on S-rich volcanism, could have been a factor in the metamorphism.

A key consideration is the high oxidation states exhibited by some large granulite-facies terranes. The principal signatures of such granulites are high Fe_2O_3 contents of ilmenite (over 50 vol. % exsolved hematite in the Wilson Lake, Labrador and Shevaroy Hills, South India areas: Currie & Gittens, 1988; Harlov *et al.*, 1997), high Mg/(Mg + Fe) ratios in the mafic minerals, indicative of Fe depletion of silicates, and the presence of Fe-deficient pyrrhotite and/or pyrite with magnetite. The Shevaroy Hills rocks are permeated with veins of pyrite + magnetite, and these two minerals without pyrrhotite accompany the highest Fe_2O_3 contents in ilmenite and the most Fe-depleted mafic silicates (Harlov *et al.*, 1997), indicating that the high oxidation state shown by many of the Shevaroy Hills granulites is a near-peak metamorphic feature. Arima *et al.* (1986), on the other hand, inferred that the great oxidation of the Wilson Lake rocks was inherited from a highly oxidized sedimentary protolith. This hypothesis could not apply to the South Indian Archean Craton, in which orthogneiss greatly exceeds metasedimentary components, especially in view of the reducing sedimentary environments that prevailed in the Late Archean (Hattori & Cameron, 1986).

Cameron & Hattori (1994) suggested a link between highly oxidized granulites and S-rich volcanism, in that both phenomena might result from the action of oxidizing late-stage magmatic fluids. The possibility that SO_2 in fluids derived from underplated magmas could have played a role in oxidation of the Shevaroy Hills granulites was suggested by Harlov *et al.* (1997, p. 714), based on the abundance of sulfide–oxide veins in these rocks. The present work introduces a modification of these ideas, in that sulfate ion, dissolved in a concentrated brine, possibly of magmatic origin, could be effective in sulfidation and oxidation reactions during deep-crustal metamorphism. Interaction of sulfate-bearing solutions with deep-crustal (i.e. granulite facies) assemblages can be modeled with the reaction

$$\underset{\text{fluid}}{CaSO_{4,aq}} + 2\underset{\text{opx}}{FeSiO_3} = \underset{\text{po}}{FeS} + \underset{\text{cpx}}{CaFeSi_2O_6} + 2O_2. \quad (4)$$

Reaction (4) implies that the assemblage orthopyroxene (opx) + clinopyroxene (cpx) + pyrrhotite (po) generates, under granulite-facies P–T conditions and high oxygen fugacity, a high activity of $CaSO_4$, which, if a fluid is present, would correspond to a $CaSO_{4,aq}$ concentration approaching anhydrite saturation. Conversely, an infiltrated metamorphic fluid with a high sulfate content, which would necessarily be highly oxidized, could serve as an agent of oxygen metasomatism. In order to coexist with the anhydrous assemblage of reaction (4) at 800°C and 10 kbar, the H_2O activity could be no higher than about 0·5, which could correspond to a NaCl mole fraction of near 0·3 (Aranovich & Newton, 1996). This solution could be very rich in $CaSO_4$, perhaps as much as 20 wt %, before anhydrite saturation would occur.

Figure 6 shows reaction (4) at 8 kbar, assuming that $X_{NaCl} = 0{\cdot}3$, X_{Fe} in ferrosilite is 0·5, X_{Fe} in hedenbergite is 0·2, pyroxene activity is the square of mole fraction, and that pyrrhotite activity is 0·875. These compositions are representative of the highest grade (Zone D) part of

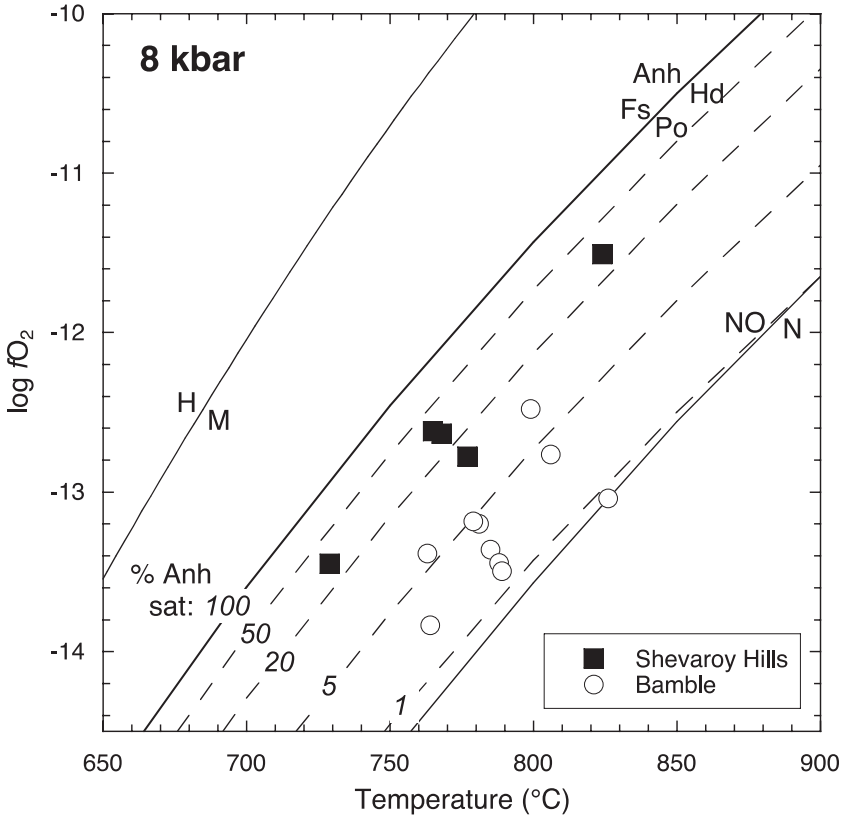

Fig. 6. $CaSO_4$ in metamorphic fluids at 8 kbar, expressed as a percentage of anhydrite saturation in a saline fluid of $X_{NaCl} = 0{\cdot}3$ (dashed lines). The array of such curves is limited at high fO_2 by anhydrite saturation [reaction (4), text]. All curves calculated using SUPCRT92 (Helgeson *et al.*, 1978; Johnson *et al.*, 1992). Anh, anhydrite; Fs, ferrosilite; Hd, hedenbergite; Po, pyrrhotite. Also plotted are the self-consistent fO_2–T points for rocks from the Bamble (South Norway; Harlov, 1992) and Shevaroy Hills (South India; Harlov *et al.*, 1997) terranes. If solute $CaSO_4$ accounts for the observed high oxidation states, the metamorphic fluids would be 1–10% $CaSO_4$-saturated for Bamble, and 15–40% $CaSO_4$-saturated for Shevaroy Hills.

the Bamble Sector, South Norway, or the Shevaroy Hills terrane, South India (Harlov, 1992; Harlov *et al.*, 1997). The curve was constructed with thermodynamic data for the minerals from SUPCRT92 (Helgeson *et al.*, 1978; Johnson *et al.*, 1992). Contours of $CaSO_4$ concentration are shown as percentages of anhydrite saturation. The calculation is quite robust, in that an uncertainty of as much as ± 20 kJ in ΔG of the reaction has only a small effect on the position of the curves. $CaSO_4$ activities are taken proportional to the squares of their concentrations, in keeping with reaction (3). Also shown in Fig. 6 are calculated oxygen fugacity and temperature data for individual rocks from the two terranes (Harlov, 1992; Harlov *et al.*, 1997).

The indication of Fig. 6 is that the fO_2–T conditions inferred for Bamble Zone D are compatible with $CaSO_4$ concentrations in aqueous fluids ranging from 1 to 10% of anhydrite saturation, and for the Shevaroy Hills of 15–40% of anhydrite saturation. The distinctly different oxidation signatures of the two terranes are not likely to result from a systematic difference in protolith oxidation, in view of the expected local variability of initial oxidation state, and in view of the more reduced nature of surficial conditions in the Archean (Hattori & Cameron, 1986), but more probably result from more consistent controls which characterized the high-grade metamorphism in the two areas. We propose that the difference in oxidation state may have resulted from unique sulfur and chlorine concentrations and oxidation states of underplated magmas in the two areas. As with Mt Pinatubo-type volcanism, the basaltic source of oxidizing volatiles must itself been very oxidized in order to accomplish major host–rock oxidation with moderate amounts of expelled fluid.

Small fluid/rock ratios are indicated by the often limited amounts of metasomatism and stable isotope homogenization observed in some granulites (Valley *et al.*, 1990). The question of whether small amounts of fluids could have accomplished the large-scale oxidation observed in some granulites is addressed quite simply by calculating the amounts of infiltrated fluids necessary to transport enough oxygen to oxidize a significant

amount, say half, of the FeO in an intermediate granulite to Fe_2O_3. For a typical Shevaroy Hills orthopyroxene-bearing orthogneiss of 5 wt % FeO, 0·56 wt % of additional oxygen must be introduced. For a NaCl-rich brine 25% saturated in anhydrite at 800°C and 8 kbar, the amount of introduced fluid of $X_{NaCl} = 0{\cdot}3$ would have to be only 9·2 wt % of the rock mass it interacts with, assuming that reaction (4) goes to completion. This small quantity is consonant with the limited amount of fluid necessary to break down biotite to orthopyroxene (Aranovich & Newton, 1998), but would be too small to produce measurable oxygen isotope shifts in rocks that are volumetrically 90% oxygen, even if the infiltrating fluid is initially far removed from isotopic equilibrium with the host rock. On the other hand, the amounts of infiltrated pure H_2O or CO_2 that would be necessary to oxidize a substantial amount of the ferrous iron in an intermediate orthogneiss would be improbably large, as the amounts of O_2 such fluids can release by dissociation at high fO_2 are minuscule (Frost, 1991). Thus, a concentrated sulfate-rich brine may be a uniquely effective vector for large-scale oxidation in the deep crust.

It is concluded that saline fluids, plausibly expelled from underplated mafic magmas, should be considered as an additional important factor in deep-crustal metamorphism. The highly variable volatile-element characteristics of mantle-derived magmas may in part account for the extremes of oxidation states observed in granulites, from the hematite-bearing granulites of Wilson Lake to the reduced granulites of the Ivrea Zone of North Italy, for which underplated magmas and their derivative saline solutions have been assigned major roles in the metamorphism (Franz & Harlov, 1998).

Scapolite granulites

The high-sulfur scapolites of some mafic and intermediate granulites are confined to terranes where paleopressures of 9 kbar or more are recorded: Nilgiri Hills, South India (Srikantappa *et al.*, 1986); Fiordland, New Zealand (Bradshaw, 1989); Kohistan Arc, Pakistan (Yoshino & Satish-Kumar, 2001); Furua Complex, Tanzania (Coolen, 1980); and in deep-crustal xenoliths in alkali basalts (Lovering & White, 1964). All of these occurrences are sulfate mizzonites of the approximate formula $3(An_{0{\cdot}6–0{\cdot}7}Ab_{0{\cdot}3–0{\cdot}4})\cdot(Cc_{0{\cdot}3–0{\cdot}7}Cs_{0{\cdot}3–0{\cdot}7})$, where An denotes $CaAl_2Si_2O_8$; Ab, $NaAlSi_3O_8$; Cc, $CaCO_3$; and Cs, $CaSO_4$. The high-S scapolites have very small NaCl contents. The restriction of mizzonite in orthogneisses to high-pressure granulites may be in part because the end-member sulfate scapolite 3An·Cs (sulfate meionite) is stable only at pressures above 10 kbar at 800°C (Goldsmith & Newton, 1977) and partly because coexistence with orthopyroxene may be limited in pressure by a decarbonation reaction similar to

$$\text{meionite}(3\text{An}\cdot\text{Cc}) + \text{orthopyroxene} = \text{garnet} + \text{clinopyroxene} + CO_2. \quad (5)$$

(Yoshino & Satish-Kumar, 2001).

The occurrence of some deep-crustal scapolites in veins (Bradshaw, 1989; Yoshino & Satish-Kumar, 2001) suggests that carbonate and sulfate were infiltrated volatiles, and carbon isotopes of these scapolites were interpreted by those workers to infer a juvenile magmatic or subcrustal origin of the volatiles. It is postulated as a consequence of the present experimental work that infiltration of sulfate and carbonate into the deep crust in a concentrated alkali chloride solution formed scapolite by reaction with intermediate plagioclase. The complex salt solution plausibly emanated from underplated basaltic magmas, which supplied the heat for metamorphism.

Existing experimental work on the stability of sulfate–carbonate mizzonite relative to plagioclase is not comprehensive enough to allow assessment of the $CaSO_4$ and $CaCO_3$ activities necessary to form scapolite in mafic to intermediate granulites at deep-crustal conditions. Goldsmith & Newton (1977) synthesized a mizzonite of equimolar Cc and Cs composition at 1100°C and 15 kbar in the presence of excess calcite and anhydrite. It has not yet been demonstrated that a low-Cl mizzonite can form from a concentrated NaCl solution undersaturated in calcite and anhydrite. Equilibria of feldspars with complex brines will be an important avenue of investigation for the future.

Porphyry Cu–Mo ore deposits

Many of the world's largest Cu–Mo sulfide ore deposits occur in the roof zones of small alkaline granite or monzonite plutons (e.g. White *et al.*, 1981). Many of the lower-temperature alteration zones have disseminated to massive anhydrite with or without hematite. Several students of these deposits believed that ore-forming fluids must have encountered evaporite sequences in order to acquire $CaSO_4$; a minority preferred orthomagmatic saline fluids as a source of $CaSO_4$. Roedder (1971) found that several of the largest porphyry ore deposits of the western United States show very concentrated brine inclusions in vein quartz from the highest-temperature, near-magmatic deposits. The ultrasaline fluid inclusions typically contain abundant halide, carbonate, sulfate, sulfide and oxide daughter minerals. Roedder (1984, table 15-5) listed many worldwide occurrences of this type of ore deposit, with descriptions of the fluid inclusions. The majority of the occurrences have highly saline inclusions containing anhydrite and hematite, often with other sulfate and sulfide minerals. Roedder (1984) explained the highly oxidized nature of

the fluid inclusions by a process of H_2 leakage out of the inclusions after entrapment, with residual oxidation.

The preceding applications of the present experimental work have emphasized a juvenile/magmatic origin of highly oxidized brines containing large amounts of sulfate. We offer an analogous interpretation for the intrusion-related sulfide ore deposits—an interpretation that explains the highly oxidized fluid inclusions as a primary, rather than a secondary, effect. The very high solubility of $CaSO_4$ in concentrated NaCl solutions at near-magmatic temperatures (>750°C) indicates that a large proportion of solute sulfur in a mafic magma would partition into an exhalative saline fluid as sulfate. Subsequent interaction of this fluid with country rocks could provoke hydrous melting to produce hypabbyssal granitic stocks or Pinatubo-type dacites. The solubility of Cl is much lower in granitic magmas than in mafic magmas (Webster *et al.*, 1999), hence the salt components (and metals) of the postulated fluid will concentrate during fluid–rock interactions as H_2O is extracted into granitic liquids. Precipitation of sulfide minerals would further increase the oxygen fugacity of the already highly oxidized fluids. An intimate connection between Pinatubo S-rich volcanism and young western Luzon porphyry ore deposits in the same area was inferred by Imai *et al.* (1996). We postulate that both phenomena could be the result of the same basalt-derived saline fluid processes manifest at different crustal levels. This conjecture is similar in principle to processes of porphyry copper mineralization envisioned by Hattori & Keith (2001).

ACKNOWLEDGEMENTS

This work was supported by National Science Foundation grants EAR-9909583 and EAR-0337170. We thank Wayne Dollase for assistance with XRD studies, and Angelo Antignano, Jorge Vazquez and George Jarzebinski for help with SEM work. *Journal of Petrology* reviewers Jim Luhr, Phil Piccoli and Jim Webster, and Editor Ron Frost gave constructive and insightful reviews, which resulted in substantial changes in this paper. We are especially indebted to Eion Cameron, who provided a knowledgeable and detailed critique of an earlier version.

REFERENCES

Aranovich, L. Y. & Newton, R. C. (1996). H_2O activity in concentrated NaCl solutions at high pressures and temperatures measured by the brucite–periclase equilibium. *Contributions to Mineralogy and Petrology* **125**, 200–212.

Aranovich, L. Y. & Newton, R. C. (1998). Reversed determination of the reaction: phlogopite + quartz = enstatite + potassium feldspar + H_2O in the ranges 750–875°C and 2–12 kbar at low H_2O activity with concentrated KCl solutions. *American Mineralogist* **83**, 193–204.

Arima, M., Kerrich, R. & Thomas, A. (1986). Sapphirine-bearing paragneiss from the northern Grenville Province in Labrador, Canada. Protolith composition and metamorphic *P–T* conditions. *Geology* **14**, 884–887.

Audétat, A., Pettke, T. & Dolejš, D. (2004). Magmatic anhydrite and calcite in the ore-forming quartz-monzodiorite magma at Santa Rita, New Mexico (USA): genetic constraints on porphyry–Cu mineralization. *Lithos* **72**, 147–161.

Baratov, R. B., Gnutenko, N. A. & Kuzemko, V. M. (1984). Regional carbonization connected with the epi-Hercynian tectogenesis in the southern Tien Shan. *Doklady Akademiia Nauk SSSR* **274**, 124–126.

Barth, A. P. & Dorais, M. J. (2000). Magmatic anhydrite in granitic rocks: first occurrence and potential petrologic consequences. *American Mineralogist* **85**, 430–435.

Belkin, H. E., DeVivo, B., Lima, A. & Torok, K. (1997). Magmatic (silicates/saline/sulfur-rich/CO_2) immiscibility and zirconium and rare-earth enrichment from alkaline magma chamber margins, evidence from Ponza island, Pontine archipelago, Italy. *European Journal of Mineralogy* **8**, 1401–1420.

Bergman, A. G. & Golubeva, M. S. (1953). Complex formation of the double hetero-ionic salt type (anhydrous kainites) in ternary reciprocal systems. *Doklady Akademiia Nauk SSSR* **89**, 471–473.

Bernard, A., Demaiffe, D., Mattielli, N. & Punongbayan, R. S. (1991). Anhydrite-bearing pumices from Mount Pinatubo: further evidence for the existence of sulfur-rich magmas. *Nature* **354**, 139–140.

Block, J. & Waters, O. B., Jr (1968). The $CaSO_4$–Na_2SO_4–NaCl–H_2O system at 25° and 100°C. *Journal of Chemical and Engineering Data* **13**, 336–344.

Blount, C. W. (1965). The solubility of anhydrite in the systems $CaSO_4$–H_2O and $CaSO_4$–NaCl–H_2O and its geologic significance. Ph.D. thesis, University of California, Los Angeles, 179 pp.

Blount, C. W. & Dickson, F.W. (1969). The solubility of anhydrite ($CaSO_4$) in NaCl–H_2O from 100 to 450°C and 1 to 1000 bars. *Geochimica et Cosmochimica Acta* **33**, 227–245.

Bohlen, S. R. (1987). Pressure–temperature–time paths and a tectonic model for the evolution of granulites. *Journal of Geology* **95**, 617–632.

Bradshaw, J. Y. (1989). Late Cretaceous vein-related garnet granulites in Fiordland, Southwest New Zealand. *Journal of Geology* **97**, 687–718.

Caciagli, N. C. & Manning, C. E. (2003). The solubility of calcite in water at 6–16 kbar and 500–800°C. *Contributions to Mineralogy and Petrology* **146**, 275–285.

Cameron, E. M. & Hattori, K. (1994). Highly oxidized deep metamorphic zones: occurrence and origin. *Mineralogical Magazine* **58A**, 142–143.

Carroll, M. R. & Rutherford, M. J. (1987). The stability of igneous anhydrite: experimental results and implications for sulfur behavior in the 1982 El Chichón trachyandesite and other evolved magmas. *Journal of Petrology* **28**, 781–801.

Coolen, J. J. M. M. M. (1980). Chemical petrology of the Furua Granulite Complex, Southern Tanzania. *Free University of Amsterdam Papers of Geology, Series 1* **13**, 1–258.

Currie, K. L. & Gittins, J. (1988). Contrasting sapphirine parageneses from Wilson Lake, Labrador and their tectonic implications. *Journal of Metamorphic Geology* **6**, 603–622.

Davies, C. W. (1962). *Ion Association*. Washington, DC: Butterworth, 190 pp.

Fein, J. B. & Walther, J. V. (1987). Calcite solubility and speciation in supercritical CO_2–H_2O fluids. *Geochimica et Cosmochimica Acta* **51**, 1665–1673.

Fein, J. B. & Walther, J. V. (1989). Calcite solubility and speciation in supercritical NaCl–HCl aqueous fluids. *Contributions to Mineralogy and Petrology* **103**, 317–324.

Franz, L. & Harlov, D. E. (1998). High-grade K-feldspar veining in granulites from the Ivrea–Verbano Zone, northern Italy: fluid flow in the lower crust and implications for granulite facies genesis. *Journal of Geology* **106**, 455–472.

Freyer, D. & Voigt, W. (2004). The measurement of sulfate mineral solubilities in the Na–K–Ca–Cl–SO_4–H_2O system at temperatures of 100, 150 and 200°C. *Geochimica et Cosmochimica Acta* **68**, 307–318.

Frost, B. R. (1991). Introduction to oxygen fugacity and its petrologic significance. *Reviews in Mineralogy* **25**, 1–9.

Frost, B. R. & Touret, J. L. R. (1989). Magmatic CO_2 and saline melts from the Sybille monzosyenite, Laramie anorthosite complex, Wyoming. *Contributions to Mineralogy and Petrology* **103**, 178–186.

Gerlach, T. M., Westrich, H. R. & Symonds, R. B. (1996). Preeruption vapor in magma of the climactic Mount Pinatubo eruption: source of the giant stratospheric sulfur dioxide cloud. In: Newhall, C. G. & Punongbayan, R. S. (eds) *Fire and Mud*. Seattle: University of Washington Press, pp. 415–433.

Goldsmith, J. R. & Newton, R. C. (1977). Scapolite–plagioclase stability relations at high pressures and temperatures in the system $NaAlSi_3O_8$–$CaAl_2Si_2O_8$–$CaCO_3$–$CaSO_4$. *American Mineralogist* **62**, 1063–1081.

Griffin, W. L., Taylor, P. N., Hakkinen, J. W., Heier, K. S., Iden, I. K., Krogh, E. J., *et al.* (1978). Archaean and Proterozoic crustal evolution in Lofoten–Vestrålen, N. Norway. *Journal of the Geological Society, London* **135**, 629–647.

Hansteen, T. H. & Burke, E. A. J. (1990). Melt–mineral–fluid interaction in the Oslo Rift, Southeast Norway: II. High-temperature fluid inclusions in the Eikern–Skrim complex. *Norges Geologiske Undersökelse Bulletin* **417**, 15–32.

Harley, S. L. (1989). The origins of granulites, a metamorphic perspective. *Geological Magazine* **126**, 215–247.

Harlov, D. E. (1992). Comparative oxygen barometry in granulites, Bamble Sector, SE Norway. *Journal of Geology* **100**, 447–464.

Harlov, D. E., Newton, R. C., Hansen, E. C. & Janardhan, A. S. (1997). Oxide and sulphide minerals in highly oxidized, Rb-depleted Archaean granulites of the Shevaroy Hills Massif, South India: oxidation states and the role of metamorphic fluids. *Journal of Metamorphic Geology* **15**, 701–717.

Hattori, K. (1993). High sulfur magma, a product of fluid discharge from underlying mafic magma: evidence from Mount Pinatubo. *Geology* **21**, 1083–1086.

Hattori, K. & Cameron, E. M. (1986). Archaean magmatic sulphate. *Nature* **319**, 45–47.

Hattori, K. H. & Keith, J. D. (2001). Contribution of mafic melt for porphyry deposits: evidence from Pinatubo and Bingham. *Mineralium Deposita* **36**, 799–806.

Helgeson, H. C., Delany, J. M., Nesbitt, H. W. & Bird, D. K. (1978). Summary and critique of the thermodynamic properties of rock-forming minerals. *American Journal of Science* **278-A**, 1–229.

Imai, A., Listanco, E. L. & Fujii, T. (1996). Highly oxidized and sulfur-rich dacitic magma: implications for metallogenesis of porphyry copper mineralization in the Western Luzon Arc. In: Newhall, F. G. & Punongbayan, R. S. (eds) *Fire and Mud*. Seattle: University of Washington Press, pp. 865–874.

Jakubowski, R. T., Fournelle, J., Welch, S., Swope, R. J. & Camus, P. (2002). Evidence for magmatic vapor deposition of anhydrite prior to the 1991 climactic eruption of Mount Pinatubo, Philippines. *American Mineralogist* **87**, 1029–1045.

Johnson, J. W., Oelkers, E. H. & Helgeson, H. C. (1992). SUPCRT92: a software package for calculating standard molal thermodynamic properties of minerals, gases, aqueous species, and reactions from 1 to 5000 bar and 0 to 1000°C. *Computers and Geosciences* **18**, 899–947.

Kilinc, I. A. & Burnham, C. W. (1972). Partitioning of chloride between a silicate melt and coexisting aqueous phase from 2 to 8 kilobars. *Economic Geology* **67**, 231–235.

Lovering, J. F. & White, A. J. R. (1964). The significance of primary scapolite in granulitic inclusions from deep-seated pipes. *Journal of Petrology* **5**, 195–218.

Lowenstern, J. B. (1994). Chlorine, fluid immiscibility, and degassing in peralkaline magmas from Pantelleria, Italy. *American Mineralogist* **79**, 353–369.

Luhr, J. F. (1990). Experimental phase relations of water- and sulfur-saturated arc magmas and the 1982 eruptions of El Chichón Volcano. *Journal of Petrology* **31**, 781–801.

Luhr, J. F., Carmichael, I. S. E. & Varekamp, J. C. (1984). The 1982 eruptions of El Chichón volcano, Chiapas, Mexico: mineralogy and petrology of the anhydrite-bearing pumices. *Journal of Volcanology and Geothermal Research* **23**, 69–108.

Marshall, W. L., Slusher, R. & Jones, E. V. (1964). Aqueous systems at high temperature XIV: solubility and thermodynamic relationships for $CaSO_4$ in NaCl–H_2O solutions from 40° to 200°C, 0 to 4 molal NaCl. *Journal of Chemical and Engineering Data* **9**, 187–191.

McInnes, B. I. A. & Cameron, E. M. (1994). Carbonated, alkaline hybridizing melts from a sub-arc environment: mantle wedge samples from the Tabar–Lihir–Tanga–Feni arc, Papua New Guinea. *Earth and Planetary Science Letters* **122**, 125–141.

Melson, W. G., Allan, J. F., Jerez, D. R., Nelen, J., Calvache, M. L., Williams, S. N., *et al.* (1990). Water contents, temperatures, and diversity of the magmas at the catastrophic eruption of Nevado del Ruiz, November 13, 1985. *Journal of Volcanology and Geothermal Research* **41**, 97–126.

Morey, G. W. & Hesselgesser, J. M. (1950). The solubilities of some minerals in super-heated steam at high pressure. *Economic Geology* **46**, 821–835.

Newton, R. C. & Manning, C. E. (2002). Experimental determination of calcite solubility in H_2O–NaCl solutions at deep crust/upper mantle pressures and temperatures: implications for metasomatic processes in shear zones. *American Mineralogist* **87**, 1401–1409.

Norton, D. (1979). Transport phenomena in hydrothermal systems: the redistribution of chemical components around cooling magmas. *Bulletin de Minéralogie* **102**, 471–486.

Pallister, J. S., Hoblitt, R. P. & Reyes, A. G. (1992). A basalt trigger for the 1991 eruptions of Pinatubo volcano? *Nature* **356**, 426–428.

Parat, F., Dungan, M. A. & Streck, M. J. (2002). Anhydrite, pyrrhotite, and sulfur-rich apatite: tracing the sulfur evolution of an Oligocene andesite (Eagle Mountain, CO, USA). *Lithos* **64**, 63–75.

Pasteris, J. D., Wopenka, B., Wang, A. & Harris, T. N. (1996). Relative timing of fluid and anhydrite saturation: another consideration in the sulfur budget of the Mount Pinatubo eruption. In: Newhall, F. G. & Punongbayan, R. S. (eds) *Fire and Mud*. Seattle: University of Washington Press, pp. 875–891.

Philippot, P. & Selverstone, J. (1991). Trace-element-rich brines in eclogite veins: implications for fluid composition and transport during subduction. *Contributions to Mineralogy and Petrology* **106**, 417–430.

Philippot, P., Chevallier, P., Chopin, C. & Dubessy, J. (1995). Fluid composition and evolution in coesite-bearing rocks (Dora Maira Massif, western Alps): implications for element recycling during subduction. *Contributions to Mineralogy and Petrology* **121**, 29–41.

Roedder, E. (1971). Fluid inclusion studies on porphyry-type ore deposits at Bingham, Utah, Butte, Montana, and Climax, Colorado. *Economic Geology* **46**, 98–120.

Roedder, E. (1984). *Fluid Inclusions*. *Reviews in Mineralogy* **12**, 1–644.

Rye, R. O., Luhr, J. F. & Wasserman, M. D. (1984). Sulfur and oxygen isotopic systematics of the 1982 eruptions of El Chichón Volcano,

Chiapas, Mexico. *Journal of Volcanology and Georthermal Research* **23**, 109–123.

Samson, M., Liu, W. & Williams-Jones, A. E. (1995). The nature of orthomagmatic fluids in the Oka carbonatite, Quebec, Canada: evidence from the fluid inclusions. *Geochimica et Cosmochimica Acta* **59**, 1963–1977.

Scaillet, B., Clemente, B., Evans, B. W. & Pichavant, M. (1998). Redox control of sulfur degassing in silicic magmas. *Journal of Geophysical Research* **103**, 23937–23949.

Shock, E. L., Helgeson, H. C. & Sverjensky, D. A. (1989). Calculation of the thermodynamic and transport properties of aqueous species at high pressures and temperatures: standard partial molal properties of inorganic neutral species. *Geochimica et Cosmochimica Acta* **53**, 2157–2183.

Shock, E. L., Sassani, D. C., Willis, M. & Sverjensky, D. A. (1997). Inorganic species in geologic fluids: correlations among standard molal thermodynamic properties of aqueous ions and hydroxide complexes. *Geochimica et Cosmochimica Acta* **61**, 907–950.

Srikantappa, C., Ashamanjari, K. G., & Janardhan, A. S. (1986). Gabbroic anorthosites from Kotagiri, Nilgiri Hills, Tamil Nadu. *Current Science* **55**, 896–898.

Streck, M. J. & Dilles, J. H. (1998). Sulfur evolution of oxidized arc magmas as recorded in apatite from a porphyry copper batholith. *Geology* **26**, 523–526.

Valley, J. W., Bohlen, S. R., Essene, E. J. & Lamb, W. (1990). Metamorphism in the Adirondacks: II. The role of fluids. *Journal of Petrology* **31**, 555–596.

Walther, J. V. & Long, M. I. (1986). Experimental determination of calcite solubilities in supercritical H_2O. *Fifth International Symposium on Water–Rock Interaction* **5**, 609–611.

Webster, J. D., Kinzler, R. J. & Mathez, E. A. (1999). Chloride and water solubility in basalt and andesite liquids and implications for magmatic degassing. *Geochimica et Cosmochimica Acta* **63**, 729–738.

White, W. H., Bookstrom, A. A., Kamilli, R. J., Ganster, M. W., Smith, R. P., Ranta, D. E., *et al.* (1981). Character and origin of climax-type molybdenum deposits. *Economic Geology 75th Anniversary Volume*, 270–316.

Yoshino, T. & Satish-Kumar, M. (2001). Origin of scapolite in deep-seated metagabbros of the Kohistan Arc, NW Himalayas. *Contributions to Mineralogy and Petrology* **140**, 511–531.